

Theory of Raman Superradiance Imaging of Condensed Bose Gases

H. Uys and P. Meystre

Department of Physics

The University of Arizona, Tucson, AZ, 85721

We investigate the off-resonant superradiant Raman scattering of light from a cigar-shaped atomic Bose-Einstein condensate. Superradiant emission has been proposed as applied to the imaging of quantum-degenerate atomic system, as it yields a stronger image contrast than conventional incoherent scattering. Our multimode theory is in good agreement with the time-dependent spatial features observed in superradiant absorption imaging, and the inclusion of quantum fluctuations in the initial stages of the superradiant emission account well for shot-to-shot fluctuations observed in experiments.

I. INTRODUCTION

Current experiments with ultracold quantum-degenerate atomic vapors rely heavily on absorption imaging as a probe. In most experiments, a probe light field is scattered incoherently from the atomic cloud, resulting in an absorption image that is a simple two-dimensional representation of the three-dimensional atomic density profile column-integrated along the direction of incidence. In recent work, Stamper-Kurn and coworkers have proposed the use of superradiant imaging as an alternative that harnesses this effect to enhance absorption image contrast [1, 2]. However, the spatial structure of the absorption image is not in this case simply proportional to the initial state atomic-density, and the resulting images need to be interpreted with care. The goal of this paper is to address this problem by presenting a detailed theory of superradiant imaging in a cigar-shaped Bose-Einstein condensate.

Superradiance is a well-known phenomenon [3] that was first discussed by Dicke [4]. In that process, atoms scatter light collectively, producing a short burst of intense radiation. In a typical superradiance experiment with Bose-Einstein condensates, an elongated sample of ultracold atoms is subjected to a pulse of far off-resonant light. For an appropriate polarization of that field, the cigar-shaped condensate geometry results in the scattering of photons predominantly into modes propagating along the long axis of the sample, commonly referred to as the end-fire-modes (EFM). For a Bose-condensed atomic cloud, the scattering process leads in addition to the coherent amplification of the recoiling atomic fields. Such coherent matter-wave amplification (CMA) has been observed both in the case of Rayleigh scattering [5, 6, 7] and of Raman scattering [8, 9], and several theoretical descriptions of this effect have been published [10, 11, 12, 13].

In two recent papers, Zobay and Nikolopoulos [14, 15] gave a detailed semiclassical analysis of the spatial features of both the matter-wave and the optical fields in CMA experiments based on Rayleigh scattering. They found that propagation effects play a crucial role in the amplification process and account for several characteristic features seen in experiments [5, 8]. These include

the characteristic “X” and fan shapes of the atomic recoil modes corresponding to the strong and weak pulse limits respectively, the asymmetry between forward and backward side-modes in the strong pulse regime, and the depletion of the condensate center in the weak pulse regime. Furthermore, they find that a minimum in superradiant emission does not necessarily imply a small EFM field inside the atomic sample, as a result of the scattering of EFM photons back into the pump beam. They also demonstrate that propagation effects lead to sub-exponential growth of the scattered fields in contrast to the exponential growth seen in fully quantized uniform field models, an effect reminiscent of laser lethargy in short-wavelength optical amplifiers [16, 17].

An important aspect of superradiance experiments is the appearance of large shot-to-shot fluctuations, a result of the quantum noise that dominates the dynamics during the initial stages of the experiment [3, 18, 19, 20]. At later times the scattered fields become macroscopically occupied and evolve in an essentially classical manner from initial conditions determined by those quantum fluctuations. A common strategy to treat the full evolution of a superradiance problem is therefore to break the problem into an initial quantum stage followed by a classical stage. The initial stage is analyzed primarily to determine the appropriate probability distribution of initial conditions for the classical stage. Experimentally observed fluctuations in the classical stage are simulated by solving the dynamics a large number of times with initial conditions chosen according to this probability distribution, each simulation representing a single realization of the experiment.

The aim of the present paper is three-fold. Firstly, we extend Refs. [14, 15] to a multimode quantum description that allows for a systematic treatment of the build-up of the classical fields from quantum noise, thereby accounting for shot-to-shot fluctuations. Secondly, whereas Refs. [14, 15] focussed on the post-pump expansion patterns of the recoiling modes to check self-consistency of their predictions, we investigate the time-dependent imaging of the condensate *while* undergoing superradiant emission under the influence of an optical pump field. Lastly, we generalize the theory to the Raman case, where the ground state of the recoiling atoms is different from

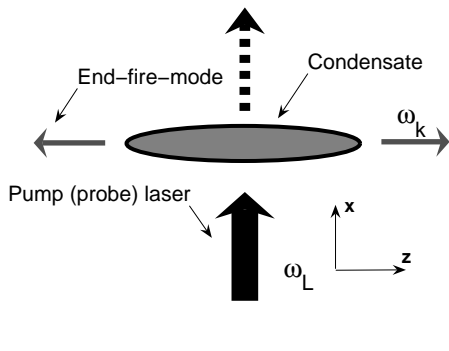
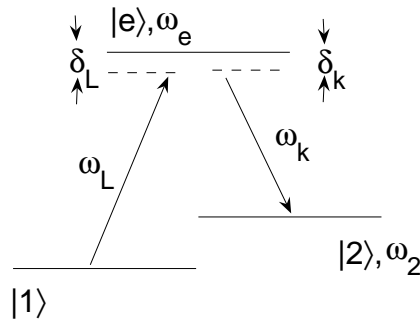


FIG. 1: Experimental setup

their initial state. As we will see, there is negligible overlap between left- and right travelling EFMs in that case, at least until the first superradiance peak, so that only the first-order forward recoiling atomic modes are typically relevant [8].

The paper is organized as follows. Section II discusses the experiment under consideration, introduces our model, and considers the initial stages of the evolution of the atoms and light field, treating the scattered optical field quantum mechanically. Section III turns then to the classical stage by solving coupled Maxwell-Schrödinger equations within the slowly varying envelope approximation. Numerical results are presented in Sec. IV, and Sec. V is a summary and conclusion.

II. INITIAL STAGE AND QUANTUM FLUCTUATIONS

We consider a cigar-shaped Bose-Einstein condensate with width w and length L . The ultracold atoms in the

condensate may undergo Raman scattering between two ground states $|1\rangle$ and $|2\rangle$ via an off-resonant excited state $|e\rangle$. The energy of level $|1\rangle$ is taken as the zero of energy, and the energies of the states $|2\rangle$ and $|e\rangle$ are $\hbar\omega_2$ and $\hbar\omega_e$, respectively, see Fig. 1. We assume that the transition $|1\rangle \rightarrow |e\rangle$ is driven by a classical pump laser $\mathbf{E}_L(t)$ of frequency ω_L and polarized along the \hat{y} -axis, with

$$\omega_L = \omega_e - \delta_L \quad (1)$$

while the transition $|e\rangle \rightarrow |2\rangle$ is via spontaneous emission to a continuum of vacuum modes with frequencies

$$\omega_k = \omega_e - \omega_2 - \delta_k. \quad (2)$$

The total electric field is then

$$\begin{aligned} \hat{\mathbf{E}} &= \mathbf{E}_L(t) + \sum_{\epsilon} \int d\mathbf{k} \hat{\mathbf{E}}_{\mathbf{k}} \\ &= \hat{\mathbf{y}} \left[E_L(t) e^{i(\mathbf{k}_L \cdot \mathbf{r} - \omega_L t)} + E_L^*(t) e^{-i(\mathbf{k}_L \cdot \mathbf{r} - \omega_L t)} \right] \\ &+ \sum_{\epsilon} \int d\mathbf{k} \left[\left(\frac{\hbar\omega_{\mathbf{k}}}{2\epsilon_0 V} \right)^{\frac{1}{2}} \hat{e}_{\mathbf{k}} \hat{a}_{\epsilon\mathbf{k}}(t) e^{i\mathbf{k} \cdot \mathbf{r}} + h.c. \right], \end{aligned}$$

where the creation operators $\hat{a}_{\epsilon\mathbf{k}}^\dagger(t)$ obey the usual bosonic commutation relations

$$[\hat{a}_{\epsilon\mathbf{k}}, \hat{a}_{\epsilon'\mathbf{k}'}^\dagger] = \delta(\mathbf{k} - \mathbf{k}') \delta_{\epsilon\epsilon'}. \quad (3)$$

The incident laser field envelope $E_L(t)$ can be taken as constant in amplitude during the initial stages of the amplification process, but its full time dependence can be accounted for in the classical stages of the evolution.

We proceed by introducing bosonic matter-field creation- and annihilation operators $\hat{\psi}_i^\dagger(\mathbf{r}, t)$, $(\hat{\psi}_i(\mathbf{r}, t))$, that create (annihilate) an atom at position \mathbf{r} in electronic state $|i\rangle = |1\rangle, |e\rangle$ or $|2\rangle$, with

$$[\hat{\psi}_i(\mathbf{r}, t), \hat{\psi}_j^\dagger(\mathbf{r}', t)] = \delta_{ij} \delta(\mathbf{r} - \mathbf{r}'), \quad (4)$$

in terms of which the Hamiltonian of the atom-field system is $\hat{H} = \hat{H}_0 + \hat{H}_c$, with

$$\hat{H}_0 = \sum_{\epsilon} \int d\mathbf{k} \hbar\omega(\mathbf{k}) \hat{a}_{\epsilon\mathbf{k}}^\dagger(t) \hat{a}_{\epsilon\mathbf{k}}(t) + \int d\mathbf{r} \left\{ \hbar\omega_e \hat{\psi}_e^\dagger(\mathbf{r}, t) \hat{\psi}_e(\mathbf{r}, t) + \hbar\omega_2 \hat{\psi}_2^\dagger(\mathbf{r}, t) \hat{\psi}_2(\mathbf{r}, t) \right\}, \quad (5)$$

and the interaction Hamiltonian

$$\hat{H}_c = - \int d\mathbf{r} \left\{ \hat{\mathbf{E}} \cdot \left[\mathbf{d}_1 \hat{\psi}_e^\dagger(\mathbf{r}, t) \hat{\psi}_1(\mathbf{r}, t) + \mathbf{d}_2 \hat{\psi}_e^\dagger(\mathbf{r}, t) \hat{\psi}_2(\mathbf{r}, t) \right] + h.c. \right\}. \quad (6)$$

describes the electric dipole interaction between the atoms and the electromagnetic field, \mathbf{d}_i being the dipole moment of the $|e\rangle \leftrightarrow |i\rangle$ transition.

We assume that the atoms are initially in their ground state $|1\rangle$, and that the pump laser is sufficiently far detuned from resonance for the excited state population to remain negligible at all times. The excited level $|e\rangle$ can then be adiabatically eliminated in the standard fashion. Thus transforming to slowly varying interaction picture

operators

$$\tilde{\psi}_1(\mathbf{r}, t) = \hat{\psi}_1(\mathbf{r}, t) \quad (7)$$

$$\tilde{\psi}_e(\mathbf{r}, t) = \hat{\psi}_e(\mathbf{r}, t) e^{i\omega_e t} \quad (8)$$

$$\tilde{\psi}_2(\mathbf{r}, t) = \hat{\psi}_2(\mathbf{r}, t) e^{i\omega_2 t}, \quad (9)$$

and performing the rotating wave approximation (RWA), yields the effective Hamiltonian

$$\tilde{H} = - \int d\mathbf{r} \left\{ g_1 |\tilde{\psi}_1(\mathbf{r}, t)|^2 + \int d\mathbf{k} g_2(\mathbf{k}) \tilde{a}_{\epsilon\mathbf{k}}^\dagger(\mathbf{r}, t) \tilde{\psi}_2^\dagger(\mathbf{r}, t) e^{i(\mathbf{k}_L - \mathbf{k}) \cdot \mathbf{r}} \tilde{\psi}_1(\mathbf{r}, t) e^{i(\delta_L - \delta_k)t} + h.c. \right\}, \quad (10)$$

where

$$g_1 = \frac{(\hat{\mathbf{y}} \cdot \mathbf{d}_1)^2}{\hbar\delta_L} |E_L|^2 \quad (11)$$

and

$$g(\mathbf{k}) = (\hat{\mathbf{y}} \cdot \mathbf{d}_1) (\hat{\epsilon} \cdot \mathbf{d}_2) \sqrt{\frac{\omega_k}{2\hbar\epsilon_0 V}} \left(\frac{\delta_k + \delta_L}{\delta_k \delta_L} \right) E_L. \quad (12)$$

In Eq. (10) we have chosen for convenience the electric field polarization axes so that one of them is aligned with the atomic dipole moment. The dot product with the orthogonal direction then vanishes and we may drop the sum over polarizations.

The effect of the Hamiltonian \tilde{H} is to transfer atoms initially in the ground state $|1\rangle$ and with spatial wave function $\phi_0(\mathbf{r})$ into the ground state $|2\rangle$ with a momentum conserving spatial wave function $\phi_0(\mathbf{r}) e^{i(\mathbf{k}_L - \mathbf{k}) \cdot \mathbf{r}}$ via scattering of a photon into mode \mathbf{k} . Following Ref. [11] we therefore expand the matter-field operators into quasi-modes according to

$$\tilde{\psi}_1(\mathbf{r}) = \phi_0(\mathbf{r}) \tilde{c}_0 \quad (13)$$

and

$$\tilde{\psi}_2(\mathbf{r}) = \int d\mathbf{q} \phi_0(\mathbf{r}) e^{i\mathbf{q} \cdot \mathbf{r}} \tilde{c}_q, \quad (14)$$

where \tilde{c}_0^\dagger creates a particle in a quasi-mode with electronic state $|1\rangle$ and wave function $\langle \mathbf{r} | 0 \rangle = \phi_0(\mathbf{r})$ and \tilde{c}_q^\dagger creates a particle in a quasi-mode with electronic state $|2\rangle$ and wave function $\langle \mathbf{r} | \mathbf{q} \rangle = \phi_0(\mathbf{r}) e^{i\mathbf{q} \cdot \mathbf{r}}$. These quasi-modes are nearly orthogonal provided that they are separated by an angle

$$\theta_\perp \gtrsim K_w / |k| = \lambda / (\pi w),$$

where $K_w = 2/w$ is the momentum width of the condensate. In that case the quasi-mode creation and annihilation operators \tilde{c}_q obey to a good approximation bosonic commutation relations

$$[\tilde{c}_q, \tilde{c}_{q'}^\dagger] \approx \delta_{qq'}. \quad (15)$$

They are therefore expected to be statistically independent during the early stages of the evolution.

In terms of the quasi-modes q , the Hamiltonian (10) becomes

$$H = 2g_1\hat{c}_0^\dagger\hat{c}_0 + \sum_{\mathbf{q}} \int d\mathbf{k} \left[\eta(\mathbf{k}, q) e^{i(\delta_L - \delta_k)t} \tilde{a}_\mathbf{k}^\dagger \hat{c}_q^\dagger \hat{c}_0 + \eta^*(\mathbf{k}, q) e^{-i(\delta_L - \delta_k)t} \hat{c}_0^\dagger \hat{c}_q a_\mathbf{k} \right] \quad (16)$$

where

$$\eta_{\mathbf{q}}(\mathbf{k}) = g(\mathbf{k}) \int d\mathbf{r} |\phi_0(\mathbf{r})|^2 e^{i(\mathbf{k}_L - \mathbf{k} - \mathbf{q}) \cdot \mathbf{r}}. \quad (17)$$

In Eqs. (16) and (17) we have neglected higher-order scattering terms, an approximation justified in the first stages of the evolution, and used the normalization condition $\int d\mathbf{r} |\phi_0(\mathbf{r})|^2 = 1$. This Hamiltonian (16) differs from the effective Hamiltonian derived by Moore and Meystre for the Rayleigh scattering case [11] in that the electronic state of recoiling atomic modes is $|2\rangle$ instead of the original ground state $|1\rangle$ and the term oscillating with frequency $\delta_L - \delta_k = \omega_k - (\omega_L - \omega_2)$ enforces the coupling of the scattered modes to photons with frequency $\omega_L - \Omega_2$ instead of ω_L .

With these differences in mind, we may easily generalize the results of Ref. [11] and determine that quasi-modes initially grow exponentially,

$$\tilde{c}_{\mathbf{q}} = \exp[G_{\mathbf{q}} N t / 2] \tilde{c}_{\mathbf{q}}(0) + \int_0^t d\tau \exp[G_{\mathbf{q}} N t / 2] \tilde{f}_{\mathbf{q}}^\dagger(t - \tau), \quad (18)$$

where

$$G_{\mathbf{q}} = 2\pi \int d\mathbf{k} |\eta_{\mathbf{q}}(\mathbf{k})|^2 \delta[\omega_k - (\omega_L - \omega_2)] \quad (19)$$

and $\tilde{f}_{\mathbf{q}}(t - \tau)$ is a noise operator of which the second-order correlation functions are given in the Markov approximation by

$$\langle \tilde{f}_{\mathbf{q}}^\dagger(t) \tilde{f}_{\mathbf{q}}(t') \rangle = 0, \quad (20)$$

$$\langle \tilde{f}_{\mathbf{q}}(t) \tilde{f}_{\mathbf{q}}^\dagger(t') \rangle = G_{\mathbf{q}} N \delta(t - t'). \quad (21)$$

In this limit, the probability $P_{\mathbf{q}}(n_q, t)$ of having n atoms in mode \mathbf{q} at time t is that of a chaotic field,

$$P_{\mathbf{q}}(n, t) = \frac{1}{\bar{n}_{\mathbf{q}}(t)} \left(1 + \frac{1}{\bar{n}_{\mathbf{q}}(t)} \right)^{-(n+1)}, \quad (22)$$

where $\bar{n}_{\mathbf{q}}(t) = \langle \tilde{c}_{\mathbf{q}}^\dagger \tilde{c}_{\mathbf{q}}(t) \rangle$ is the mean number of atoms in the quasi-mode q at time t .

An important feature of the linear gain factor $G_{\mathbf{q}}$ is that it remains relatively constant for quasi-modes excited via the scattering of photons at small angles $\theta_{\mathbf{k}}$ with respect to the long axis of the condensate. This is the case until $\theta_{\mathbf{k}}$ reaches the geometric angle

$$\theta_g \approx \frac{w}{L}$$

after which the linear gain $G_{\mathbf{q}}$ falls off rapidly. The electromagnetic modes corresponding to scattering into that

angle collectively form the EFM, and they dominate the short-time dynamics of the system.

This suggests that we may accurately simulate the linear dynamics of the superradiant system by considering the scattering of photons into a finite number of modes distributed within a solid angle $2\pi\theta_g$ around the long axis of the condensate only. We note that while the geometric angle into which significant scattering takes place, is fixed by the aspect ratio of the condensate, the number m of independent quasi-modes depends also on the wavelength of the optical fields involved,

$$m \approx \left(\frac{\theta_g}{\theta_{\perp}} \right)^2 = \left(\frac{\pi w^2}{\lambda L} \right)^2 = F^2, \quad (23)$$

where F is the Fresnel number. Typical experiments correspond to a number of quasi-modes $m \approx 10 \sim 10^2$.

III. CLASSICAL EVOLUTION

We now turn to the quantum-noise initiated classical regime that occurs once the superradiance process is fully initiated and the scattered modes are macroscopically occupied. In that regime the optical field can be described classically as

$$\begin{aligned} \mathbf{E}_{cl} &= \mathbf{E}_L + \sum_{\mathbf{k}} \mathbf{E}_{\mathbf{k}} \\ &= \hat{\mathbf{y}} \left[E_L(\mathbf{r}, t) e^{i(\mathbf{k}_L \cdot \mathbf{r} - \omega_L t)} + E_L^*(\mathbf{r}, t) e^{-i(\mathbf{k}_L \cdot \mathbf{r} - \omega_L t)} \right] \\ &+ \hat{\mathbf{y}} \sum_{\mathbf{k}} \left[E_{\mathbf{k}}(\mathbf{r}, t) e^{i(\mathbf{k} \cdot \mathbf{r} - \omega_k t)} + E_{\mathbf{k}}^*(\mathbf{r}, t) e^{-i(\mathbf{k} \cdot \mathbf{r} - \omega_k t)} \right]. \end{aligned}$$

Following the discussion of Sec. II we restrict the sum over \mathbf{k} to the discrete set of quasi-modes in the end-fire cone and set $\omega_k = \omega_L - \omega_2$. At this point we also assume that pump field is no longer undepleted. As usual, the field amplitudes $E_i(\mathbf{r}, t)$ are assumed to be slowly varying,

$$|\nabla E_i(\mathbf{r}, t)| \ll |k_i E_i(\mathbf{r}, t)|, \quad (24)$$

$$\left| \frac{\partial E_i(\mathbf{r}, t)}{\partial t} \right| \ll |\omega_i E_i(\mathbf{r}, t)|. \quad (25)$$

Eliminating adiabatically the excited electronic state of the atoms as before and introducing the slowly varying Schrödinger field operators

$$\tilde{\psi}_1(\mathbf{r}, t) = \hat{\psi}_1(\mathbf{r}, t) \quad (26)$$

$$\tilde{\psi}_e(\mathbf{r}, t) = \hat{\psi}_e(\mathbf{r}, t) e^{i\omega_e t} e^{-i\mathbf{k}_L \cdot \mathbf{r}} \quad (27)$$

$$\tilde{\psi}_{\mathbf{k}}(\mathbf{r}, t) = \hat{\psi}_{\mathbf{k}}(\mathbf{r}, t) e^{i\omega_2 t} e^{-i(\mathbf{k}_L \cdot \mathbf{r} - \mathbf{k} \cdot \mathbf{r})}. \quad (28)$$

results in the effective Hamiltonian

$$\tilde{H} = - \int d\mathbf{r} \left\{ g_1 |\tilde{\psi}_1(\mathbf{r}, t)|^2 + \sum_{\mathbf{k}} g_{\mathbf{k}} \tilde{\psi}_{-\mathbf{k}}^\dagger(\mathbf{r}, t) \tilde{\psi}_1(\mathbf{r}, t) + h.c. \right\}, \quad (29)$$

where

$$g_{\mathbf{k}} = \frac{d_1 d_2}{\delta_L \hbar} E_{\mathbf{k}}^* E_1. \quad (30)$$

In Eq. (30) we have taken the atomic dipoles to be aligned with the electric field vector and have neglected its variation in \mathbf{k} over the geometric angle. For the Raman system under consideration we need not include higher-order modes of the form $\tilde{\psi}_{i\mathbf{k}_L+j\mathbf{k}}$ (i, j being integers) in the sum over \mathbf{k} , as would be necessary for the case of Rayleigh scattering.

The Hamiltonian (29) yields the matter-wave Heisenberg equations of motion

$$\frac{d\Psi_1(\mathbf{r}, t)}{d\tau} = i \left(\frac{\Omega_L}{\delta_L} \right) \mathcal{E}_1^* \left[\mathcal{E}_1 \Psi_1 + \sum_{\mathbf{k}} \mathcal{E}_{\mathbf{k}} \Psi_{-\mathbf{k}} \right] \quad (31)$$

$$\frac{d\Psi_{\mathbf{k}}(\mathbf{r}, t)}{d\tau} = i \left(\frac{\Omega_L}{\delta_L} \right) \mathcal{E}_{-\mathbf{k}}^* \left[\mathcal{E}_1 \Psi_1 + \sum_{\mathbf{k}} \mathcal{E}_{\mathbf{k}} \Psi_{-\mathbf{k}} \right], \quad (32)$$

Where we have cast all matter- and electric fields in dimensionless form by approximating $d_1 \approx d_2 \approx d$ and defined the characteristic Rabi frequency

$$\Omega_L = \frac{dE_L^{\text{in}}}{\hbar}, \quad (33)$$

where E_L^{in} is the incident amplitude of the pump laser field, the characteristic density

$$\rho_c = \frac{N}{Lw^2}, \quad (34)$$

the dimensionless field amplitudes

$$\mathcal{E}_i = \frac{E_i}{E_L^{\text{in}}}, \quad (35)$$

and

$$\Psi_i = \frac{\tilde{\psi}_i}{\sqrt{\rho_c}}, \quad (36)$$

and the dimensionless time is $\tau = \Omega_L t$.

The electric field is governed by the Maxwell wave equation

$$\nabla \times \nabla \times \mathbf{E} + \frac{1}{c^2} \frac{\partial^2 \mathbf{E}}{\partial t^2} = - \frac{1}{c^2 \epsilon_0} \frac{\partial^2 \mathbf{P}}{\partial t^2}, \quad (37)$$

where \mathbf{P} is the macroscopic polarization of the medium,

$$\mathbf{P} = \mathbf{d}_1 \hat{\psi}_e^\dagger \hat{\psi}_1 + \sum_{\mathbf{k}} \mathbf{d}_2 \hat{\psi}_e^\dagger \hat{\psi}_{\mathbf{k}} + h.c. \quad (38)$$

With $\nabla \times \nabla \times \mathbf{a} = \nabla(\nabla \cdot \mathbf{a}) - \nabla^2 \mathbf{a}$ and exploiting the fact that the divergence of the electric field must vanish in the absence of free sources the wave equation takes the familiar form

$$\nabla^2 \mathbf{E} - \frac{1}{c^2} \frac{\partial^2 \mathbf{E}}{\partial t^2} = \frac{1}{c^2 \epsilon_0} \frac{\partial^2 \mathbf{P}}{\partial t^2}. \quad (39)$$

Since the geometric angle is small we treat for simplicity all EFM as propagating in a direction parallel to the long axis z of the condensate and henceforth treat the electric field momenta as scalars $\pm k$. In addition, the propagation time of the light fields through the condensate is extremely short compared to all other characteristic times of the system. It follows that if the atomic system is pumped by a pulse of duration long compared to that time, the electric fields adiabatically follow the atomic fields and we can safely eliminate the partial time derivatives in the slowly varying Maxwell wave equation. Eliminating $\hat{\psi}_e$ in the polarization and within the slowly varying envelope approximation we have then

$$\frac{\partial \mathcal{E}_L}{\partial \xi} = i \aleph \Psi_1^\dagger \left\{ \mathcal{E}_1 \Psi_1 + \sum_k \mathcal{E}_k \Psi_{-k} \right\} \quad (40)$$

$$\text{sign}(k) \frac{\partial \mathcal{E}_k}{\partial \zeta} = i \aleph \Psi_{-k}^\dagger \left\{ \mathcal{E}_1 \Psi_1 + \sum_k \mathcal{E}_k \Psi_{-k} \right\}. \quad (41)$$

where $\xi = x/L$, $\zeta = z/L$ and

$$\aleph = \frac{d^2 \rho_c}{\epsilon_0 \hbar \delta_L} \frac{L}{\lambda}. \quad (42)$$

Equations (40) and (41) together with Eqns. (31) and (32), fully describe the multimode dynamics of the slowly varying envelopes of the electric- and matter-wave fields. They may be solved analytically in the short-time regime and we find that the fields $\Psi_{\pm k}$ obey the same non-exponential growth as obtained in Ref. [15],

$$\tilde{\Psi}_k(z, t) \approx \frac{\psi_0}{\sqrt{4\pi(\alpha z t)^{\frac{1}{4}}}} e^{2\sqrt{\alpha z t}}, \quad (43)$$

where $\alpha = \frac{\Omega_L \aleph}{\delta}$ and ψ_0 is the square root of the recoiling mode density at $t = 0$.

IV. NUMERICAL RESULTS

This section presents selected results from numerical simulations of the onset and growth of superradiant scattering in a cigar-shaped condensate. We assume here that all atoms in the condensate at temperature $T = 0$ are initially in the electronic ground state $|1\rangle$, and approximate their center-of-mass wave function by a gaussian. As we have seen, the amplitudes of the end-fire modes at the onset of classical regime are stochastic variables whose values must be selected at random from run-to-run to be consistent with the results of Sec II.

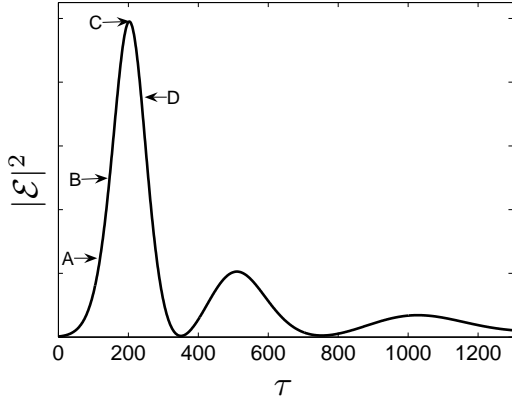


FIG. 2: Typical time evolution of the end fire modes intensity. The letters label the times at which selected density profiles are plotted in Fig. 3. The parameters used in this simulation were $\Omega_L/\delta_L = 0.2$ and $\aleph = 0.01$.

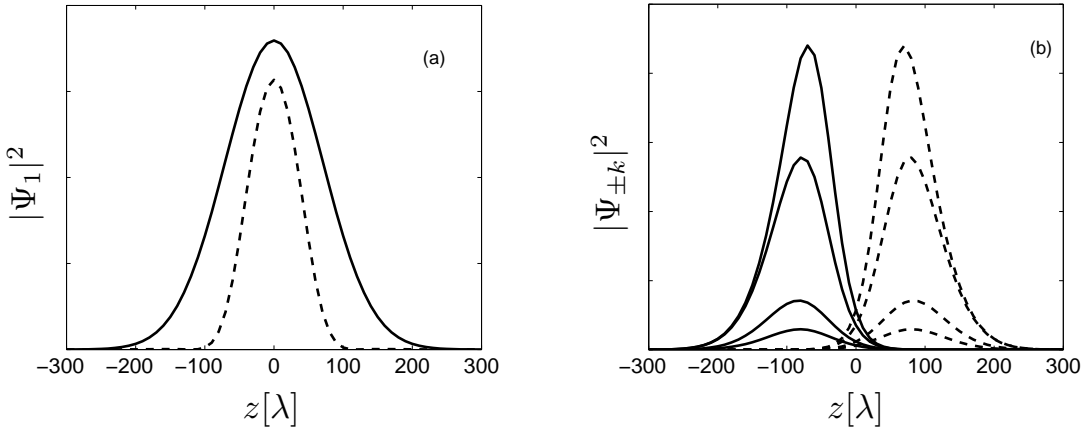


FIG. 3: (a) Density profile of the atoms in the electronic ground state $|\Psi_1\rangle$, $|\Psi_1|^2$ at $t = 0$ (solid line) and at time D of Fig. 2 (dashed line); (b) density profile of $\Psi_{\pm k}$. The solid lines are for the right-recoiling and the dashed lines for left-recoiling side modes at times A-D of Fig. 2.

To set the stage for our discussion we consider first a simplified situation with only one left-recoiling and one right-recoiling side-mode of equal initial amplitudes small compared to the amplitude of Ψ_1 , but with the same spatial structure.

Figure 2 illustrates a rather typical example of a superradiant EFM pulse shape [3], with its characteristic ringing, and Figs. 3-5 show the spatial profiles of matter- and electric fields at selected times (labelled A-D in Fig. 2) during that pulse. Of particular interest is the growth in the counterpropagating matter-wave modes $|\Psi_k|^2$ (solid line) and $|\Psi_{-k}|^2$ (dashed line) corresponding to atoms in the electronic ground state $|\Psi_2\rangle$, see Fig. 3b. These modes grow from the left- and right edges of the peak density of $|\Psi_1|^2$, a consequence of the fact that the corresponding EFM electric field builds up asymmetrically as it moves across the condensate. The overlap between counterpropagating modes is small and justifies the restriction to first-order recoiling modes. The electric field build-up is illustrated in Fig. 4 for the left-moving EFM.

The dotted horizontal line in Fig. (4) is a guide for the eye and shows that the EFM field at time D peaks along the condensate axis before diminishing to its final amplitude. This peak arises when the EFM field intensity is strong enough to allow it to be scattered back into the probe beam. As pointed out in Ref. [15] this may cause a strong EFM field to exist within the atomic system despite small emission outside the sample.

In the limit of weak absorption, the absorption of the incident laser field along the x -axis is given by

$$\alpha(x, z) \approx 1 - \frac{|E_L(x, z)|^2}{|E_L^{\text{in}}|^2}.$$

Figure 5 shows $\alpha(z) \equiv \alpha(x \gg w, z)$ after the laser field exits the condensate, for the times A-D of Fig. 2. It exhibits a double-peaked structure that tends to narrow as time increases, a consequence of the EFM photons being backscattered into the probe beam. This absorption shape appears to be in good qualitative agreement with the experimental observations of Stamper-Kurn and

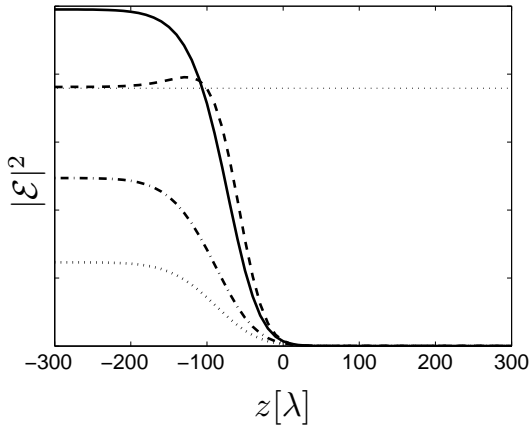


FIG. 4: Typical envelopes of EFM electric fields at times A (dotted line), B (dot-dashed line), C (solid line), and D (dashed line) of Fig. (2). The peak in intensity at time D arises when the EFM field intensity is high enough to allow scattering back into the probe beam.

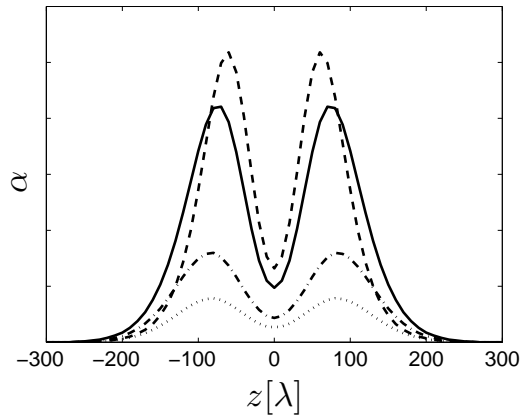


FIG. 5: Absorption profile of the pump pulse along the z axis at times A (dotted line), B (dot-dashed line), C (solid line), and D (dashed line) of Fig. 2. Note the narrowing of the double-peak structure, which occurs when atoms in electronic ground state $|2\rangle$ scatter photons back in to the probe beam in regions of high EFM field intensity.

coworkers, and clearly evidences that superradiant emission into the end-fire modes results in an absorption image that is not simply proportional to the condensate density and needs to be interpreted with care.

We now turn to the shot-to-shot fluctuations resulting from the quantum noise-dominated early stages of the emission process. To this end we solve the multimode Eqs. (31)-(32) and (40)-(41) with the initial amplitude of each quasi-mode chosen from the probability distribution (22) independently of the other modes. The average particle number \bar{n}_q is taken to be the same for all distributions.

Figures 6 (a)-(b) show absorption profiles for two randomly chosen realizations of a superradiance experiment for systems with (a) $m = 5$ and (b) $m = 20$ quasi-modes

each in the left- and right EFM directions of propagation. The asymmetry between the positive and negative z directions is very typical of all realizations. In all cases the absorption profile is shown at the time of the first peak in intensity and averaged over all modes in either the left- or right traveling EFM. The separation $\Delta\alpha$, as indicated by the dotted lines in (a), may be used to characterize the asymmetry.

Figure 6 (c)-(d) shows a false color plot constructed from 1000 realizations of the superradiance experiment for (c) $m = 5$ and (d) $m = 20$ quasi-modes each in the left- and right travelling EFMs. The profile is again taken at the first peak of the superradiant pulse. The gray scale represents the frequency of occurrence of absorption, with darkest shade of gray being the highest frequency. An important consequence of the multimode model is that on average the maximum absorption at the center of the condensate increases relative to the peak absorption with increasing number of quasi-modes. This is apparent from comparing Figs. 6 (c) and (d).

The distribution of absorption asymmetries, $\Delta\alpha$, for a random set of 1000 realizations of the experiment is plotted in Fig. 7 for $m = 1$ (gray line), $m = 5$ (broken line) and $m = 20$ (black line) quasi-modes each in the left- and right EFM directions. The width of the distribution clearly decreases with increasing number of modes. In fact, from the central limit theorem [21] the width is expected to scale as the inverse square root $1/F$ of the number of modes. This is confirmed in the insert in Fig. 7 which plots the width of distributions with $m = 5$, $m = 10$ and $m = 20$. Because of this dependence, fluctuations can be reduced by increasing the size of the condensate while keeping the aspect ratio fixed.

V. CONCLUSION

We have presented a multi-mode model of Raman superradiance imaging of Bose-condensates. The superradiant scattering into end-fire-modes was seen to lead to non-trivial, time-dependent, spatial structure in both matter- and photon fields. The microscopic quantum fluctuations that trigger the initial superradiant dynamics lead to macroscopic fluctuations and asymmetries in the spatial features of absorption images during later stages. We also showed that the multimode structure of the superradiant end-fire modes washes out spatial features in the absorption profiles, while at the same time suppressing fluctuations.

This absorption shape appears to be in good qualitative agreement with the experimental observations of Stamper-Kurn and coworkers, and clearly evidences that superradiant emission into the end-fire modes results in an absorption image that is not simply proportional to the condensate density, but contains information about the build-up and propagation of side-modes in the condensate, and needs to be interpreted with care. Future work will extend this analysis to the study of higher-order

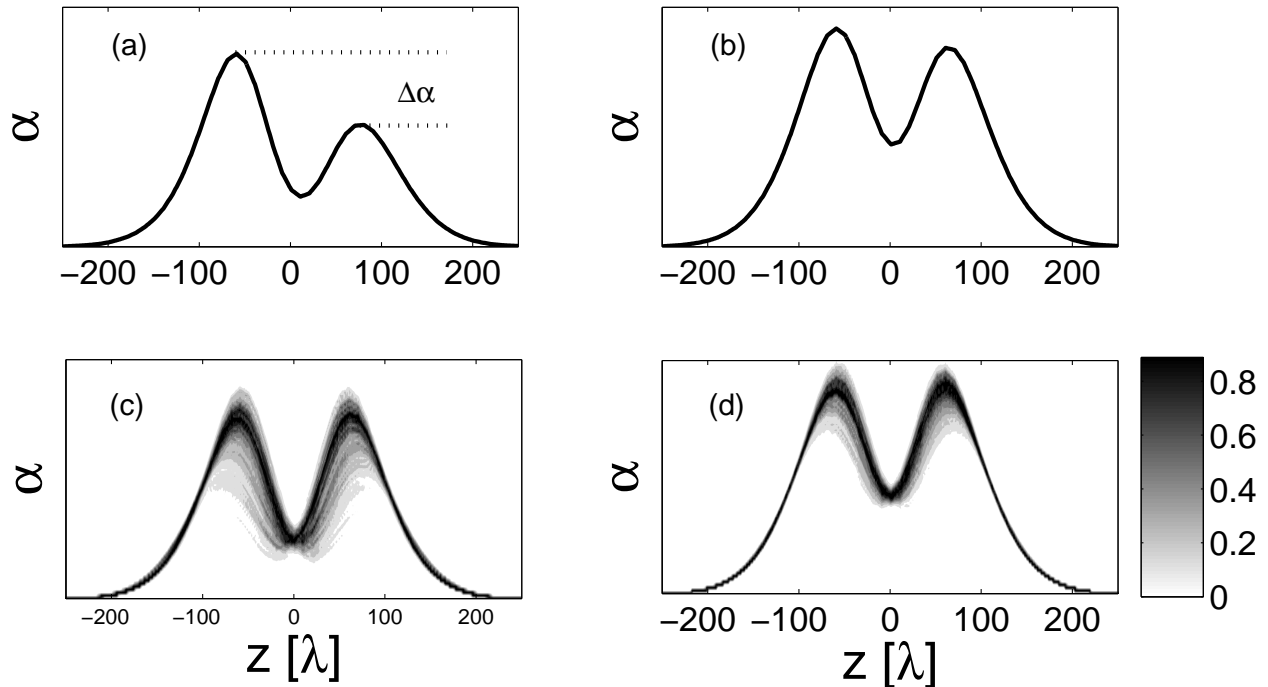


FIG. 6: Absorption profile $\alpha(z)$ of the input laser field. Figures (a)-(b) are representative profiles resulting from single realizations of a superradiance experiment for geometries with (a) $m = 5$ and (b) $m = 20$ quasi-modes each in the left- and right EFM directions. The peak separation, $\Delta\alpha$, as indicated by the dotted lines in (a) characterizes the asymmetry. Figures (c) and (d) give the frequency of occurrence of the absorption profiles resulting from 1000 realizations for (c) $m = 5$ and (d) $m = 20$. As indicated by the gray scale in the color bar, the darkest shade of gray corresponds to the most frequent occurrences.

correlations of the end-fire modes and of the quantum correlations between the optical and matter-wave fields, as well as to the case of Fermi systems.

This work is supported in part by the US Army Research Office, NASA, the National Science Foundation and the US Office of Naval Research.

Acknowledgments

We thank D. Stamper-Kurn, for making his experimental results available prior to publication.

[1] D. M. Stamper-Kurn, University of California, Berkeley (2005), private communication.

[2] L. Sadler, University of California, Berkeley (2005), division of Atomic, Molecular, and Optical Physics Conference, American Physical Society.

[3] M. Gross and S. Haroche, Phys. Rep. **93**, 301 (1982).

[4] R. H. Dicke, Phys. Rev. **93**, 99 (1954).

[5] S. Inouye, A. P. Chikkatur, D. M. Stamper-Kurn, J. Stenger, D. E. Pritchard, and W. Ketterle, Science **285**, 571 (1999).

[6] S. Inouye, T. Pfau, S. Gupta, A. P. Chikkatur, A. Görlitz, D. E. Pritchard, and W. Ketterle, Nature **402**, 641 (1999).

[7] D. Schneble, Y. Torii, M. Boyd, E. W. Streed, D. E. Pritchard, and W. Ketterle, Science **300**, 475 (2003).

[8] D. Schneble, K. C. Gretchen, W. S. Erik, B. Micah, D. E. Pritchard, and W. Ketterle, Phys. Rev. A **69**, 041601(R) (2004).

[9] Y. Yoshikawa, T. Sugiura, Y. Torii, and T. Kuga, Phys. Rev. A **69**, 041603(R) (2004).

[10] K. V. Krutitsky, F. Burgbacher, and J. Audretsch, Phys. Rev. A **59**, 1517 (1999).

[11] M. G. Moore and P. Meystre, Phys. Rev. Lett. **83**, 5202 (1999).

[12] Ö. E. Müstecaplıoglu and L. You, Phys. Rev. A **62**, 063615 (2000).

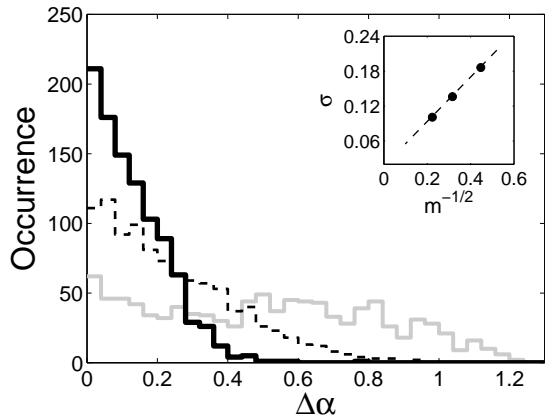


FIG. 7: Distribution of the asymmetry of absorption peaks from 1000 realizations, for systems with $m = 1$ (gray line), $m = 5$ (broken line) and $m = 20$ (black line) quasi-modes in both the left- and right EFM directions. The insert shows the scaling of the width of these distributions for $m = 5$, $m = 10$ and $m = 20$, and clearly obeys the expected $1/\sqrt{m}$ scaling.

- [13] M. M. Cola and N. Piovella, *Phys Rev. A* **70**, 045601 (2004).
- [14] O. Zobay and G. M. Nikolopoulos, *Phys. Rev. A* **72**, 041604(R) (2005).
- [15] O. Zobay and G. M. Nikolopoulos, *Phys. Rev. A* **73**, 013620 (2006).
- [16] F. A. Hopf and P. Meystre, *Physical Review A* **12**, 2534 (1975).
- [17] F. A. Hopf, P. Meystre, and D. W. McLaughlin, *Physical Review A* **13**, 777 (1976).
- [18] F. Haake, J. W. Haus, H. King, G. Schröder, and R. Glauber, *Phys. Rev. A* **23**, 1322 (1981).
- [19] I. E. Antoniou, V. V. Kocharovskiy, V. L. V. Kocharovskiy, Y. M. Mironov, and I. A. Shereshevsky, *Computer Math. Applic.* **34**, 751 (1997).
- [20] F. E. van Dorsselaer and G. Nienhuis, *Phys. Rev. A* **56**, 958 (1997).
- [21] N. G. van Kampen, *Stochastic Processes in Physics and Chemistry* (North-Holland Publishing company, 1981).